Contents

1 Quantum, classical and semiclassical analyses of photon statistics in harmonic generation†

JIŘÍ BAJER[1] and ADAM MIRANOWICZ[2,3]

[1] Department of Optics, Palacký University, 17. listopadu 50, 772 00 Olomouc, Czech Republic

[2] CREST Research Team for Interacting Carrier Electronics, School of Advanced Sciences, The Graduate University for Advanced Studies (SOKEN), Hayama, Kanagawa 240-0193, Japan

[3] Nonlinear Optics Division, Institute of Physics, Adam Mickiewicz University, 61-614 Poznań, Poland

1.1 INTRODUCTION

Harmonic generation is one of the earliest discovered and studied nonlinear optical processes. For 40 years, since the first experimental demonstration of second-harmonic generation (SHG) by Franken and co-workers [1] followed by its rigorous theoretical description by Bloembergen and Pershan [2], the harmonic generation has unceasingly been attracting much attention [3]. In particular, harmonic generation has been applied as a source of nonclassical radiation (see references [4, 5] for a detailed account and bibliography). It was demonstrated that photon antibunched and sub-Poissonian light [6, 7], as well as second [8] and higher order [9, 10] squeezed light can be produced in SHG. In experimental schemes, second-harmonic generation is usually applied for the sub-Poissonian and photon-antibunched light production, whereas second-subharmonic generation (also referred to as the two-photon down conversion) is used for the squeezed-light generation [4, 11]. Non-classical effects

† To appear in *Modern Nonlinear Optics*, ed. M. Evans, *Advances in Chemical Physics*, vol. 119(I) (Wiley, New York, 2001). This is a part of the chapter on *Nonlinear phenomena in quantum optics* by J. Bajer, M. Dušek, J. Fiurásek, Z. Hradil, A. Lukš, V. Peřinová, J. Rehácek, J. Peřina, O. Haderka, M. Hendrych, J. Peřina, Jr., N. Imoto, M. Koashi, and A. Miranowicz.

in higher-harmonic generation have also been investigated, including sub-Poissonian photocount statistics [5, 7, 12, 13], squeezing [5, 14, 15], higher-order squeezing [16, 17] according to the Hong-Mandel definition [9] or higher-power-amplitude squeezing [18, 17] based on Hillery's concept [10]. In this contribution, we will study photocount statistics of second and higher harmonic generations with coherent light inputs.

Photocount noise of the observed statistics can simply be described by the (quantum) *Fano factor* [22]

$$F^{\mathrm{Q}} \equiv \frac{\langle (\Delta\hat{n})^2 \rangle}{\langle \hat{n} \rangle} = \frac{\langle \hat{n}^2 \rangle - \langle \hat{n} \rangle^2}{\langle \hat{n} \rangle}, \tag{1.1}$$

where $\langle \hat{n} \rangle$ is the (ensemble) mean number of detected photons and $\langle (\Delta\hat{n})^2 \rangle$ is the variance of photon number. We also analyze the global (quantum) Fano factor defined to be [23]:

$$F^{\mathrm{G}} \equiv \frac{\langle\langle (\Delta\hat{n})^2 \rangle\rangle}{\langle\langle \hat{n} \rangle\rangle} = \frac{\langle\langle \hat{n}^2 \rangle\rangle - \langle\langle \hat{n} \rangle\rangle^2}{\langle\langle \hat{n} \rangle\rangle}, \tag{1.2}$$

where the mean values $\langle\langle \hat{n}^k \rangle\rangle$ are obtained by the ensemble and time averaging, i.e.,

$$\langle\langle \hat{n}^k \rangle\rangle = \lim_{T\to\infty} \frac{1}{T} \int_0^T \langle \hat{n}^k(t) \rangle dt. \tag{1.3}$$

In classical trajectory approach, the Fano factor is defined to be

$$F^{\mathrm{S}} \equiv \frac{\overline{(\Delta n)^2}}{\overline{n}} = \frac{\overline{n^2} - \overline{n}^2}{\overline{n}}, \tag{1.4}$$

as a semiclassical analogue of the quantum Fano factor. The mean values $\overline{n^k}$ in Eq. (1.4) are obtained by averaging over all classical trajectories as will be discussed in detail in Sects. 1.2.3 and 1.3.3.

Coherent (ideal laser) light has Poissonian photon-number distribution thus described by the unit Fano factor. For $F < 1$, the light is referred to as *sub-Poissonian* since its photocount noise is smaller than that of coherent light with the same intensity. Whereas for $F > 1$, the light is called *super-Poissonian* with the photocount noise higher than that for coherent light.

We shall compare different descriptions of photon-number statistics in harmonic generation within quantum, classical and semiclassical approaches. First, we will study the exact quantum evolution of the harmonic generation process by applying numerical methods including those of Hamiltonian diagonalization and global characteristics. As a brief introduction, we will show explicitly that harmonic generation can indeed serve as a source of nonclassical light. Then, we will demonstrate that the quasi-stationary sub-Poissonian light can be generated in these quantum processes under conditions corresponding to the so-called no-energy-transfer regime known in classical nonlinear optics. By applying method of classical trajectories, we will

demonstrate that the analytical predictions of the Fano factors are in good agreement with the quantum results. On comparing second [19], third [20] and higher [21] harmonic generations in the no-energy-transfer regime, we will show that the highest noise reduction is achieved in third-harmonic generation with the Fano-factor of the third harmonic equal to $F_3^{\rm Q} \approx F_3^{\rm S} = 13/16$.

1.2 SECOND-HARMONIC GENERATION

1.2.1 Quantum analysis

The quantum process of second-harmonic generation (SHG) can be described by the following interaction Hamiltonian [4, 5]:

$$\hat{H} = \hbar g \left(\hat{a}_1^2 \hat{a}_2^\dagger + \hat{a}_1^{\dagger 2} \hat{a}_2 \right), \tag{1.5}$$

where $\hat{a}_1$ and $\hat{a}_2$ denote annihilation operators of the fundamental and second-harmonic modes, respectively; g is a nonlinear coupling parameter. The Hamiltonian (1.5) describes a process of absorption of two photons at frequency ω_1 and simultaneous creation of a new photon at the harmonic frequency $\omega_2 = 2\omega_1$, together with the inverse process. Unfortunately, no exact solution of quantum dynamics of the model, described by (1.5), can be found. Thus, various analytical approximations or numerical methods have to be applied in the analysis of the conversion efficiency, quantum noise statistics or other characteristics of the process [5]. Due to mathematical complexity of the problem, the investigations of nonclassical effects in harmonic generation have usually been restricted to the regime of short interactions (short optical paths or short times). Theoretical predictions of quantum parameters (including the Fano factor or, equivalently, the Mandel Q-parameter) were obtained under the short time approximation only (see, e.g., [4, 5, 13]). This is a physically sound approximation in case of weak nonlinear coupling of optical fields. The Fano factors under the short-time approximation (i.e., for $gt \ll 1$) for coherent inputs $\alpha_1 = r_1 \exp(i\phi_1)$ and $\alpha_2 = r_2 \exp(i\phi_2)$ are given by the expansions (for $r_1, r_2 \neq 0$):

$$\begin{aligned} F_1^{\rm Q} &= 1 - 4 \sin\theta \; r_2 gt \\ &\quad + \left\{ 4 r_1^{-2} r_2^2 - 2 r_1^2 + 8[2 + \cos(2\theta)] r_2^2 \right\} (gt)^2 + \mathcal{O}\{(gt)^3\}, \\ F_2^{\rm Q} &= 1 - \frac{16}{3} \sin\theta \; r_1^2 r_2 (gt)^3 \\ &\quad + \frac{4}{3} \left\{ 2 r_2^2 + 16 r_1^2 r_2^2 - [4 + 3\cos(2\theta)] r_1^4 \right\} (gt)^4 + \mathcal{O}\{(gt)^5\}, \end{aligned} \tag{1.6}$$

where $\theta = 2\phi_1 - \phi_2$ and $\mathcal{O}\{x\}$ denotes the order of magnitude. Eq. (1.6) determines whether the generation of harmonics ($\omega + \omega \to 2\omega$) or subharmonics ($2\omega \to \omega + \omega$) occurs. It also determines the sub-Poissonian or super-Poissonian photon-number statistics of light generated during the short-time interactions. For spontaneous SHG

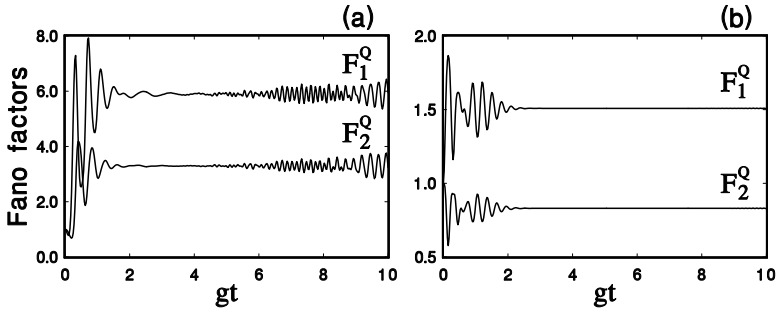

Fig. 1.1 Fano factors of the fundamental, $F_1^{\rm Q}$, and the second-harmonic mode, $F_2^{\rm Q}$, in the long-time interaction for initial coherent states with real amplitudes **(a)** $\alpha_1 = 6, \alpha_2 = 1$, and **(b)** $\alpha_1 = 6, \alpha_2 = 3$. Case **(a)** is a typical example of super-Poissonian behavior in both modes outside the no-energy-transfer regime. In case **(b)**, the harmonic mode exhibits stable sub-Poissonian statistics with $F_2^{\rm Q} \simeq 0.83$. It is a characteristic example of the sub-Poissonian behavior within the no-energy-transfer regime along the line $|\alpha_1| = 2|\alpha_2|$.

process (i.e., for $r_2 = 0$), the well-known expansions for the quantum Fano factors are

$$\begin{aligned} F_1^{\rm Q} &= 1 - 2(r_1 gt)^2 + \frac{4}{3} r_1^2 \left(3r_1^2 + 1\right) (gt)^4 + \mathcal{O}\{(gt)^6\}, \\ F_2^{\rm Q} &= 1 - \frac{4}{3}(r_1 gt)^4 + \frac{4}{45} r_1^4 \left(36 r_1^2 + 17\right) (gt)^6 + \mathcal{O}\{(gt)^8\}, \end{aligned} \tag{1.7}$$

or, equivalently, for the normally-ordered photon-number variances [6, 7, 4]:

$$\begin{aligned} \langle : (\Delta \hat{n}_1)^2 : \rangle &\equiv \langle (\Delta \hat{n}_1)^2 \rangle - \langle \hat{n}_1 \rangle = -2 r_1^4 (gt)^2 + \mathcal{O}\{(gt)^4\}, \\ \langle : (\Delta \hat{n}_2)^2 : \rangle &\equiv \langle (\Delta \hat{n}_2)^2 \rangle - \langle \hat{n}_2 \rangle = -\frac{4}{3} r_1^8 (gt)^6 + \mathcal{O}\{(gt)^8\}. \end{aligned} \tag{1.8}$$

It is seen that the photon-number statistics of fundamental mode exhibits, in the short-time regime, much stronger sub-Poissonian behavior than that of harmonic mode.

For longer interaction times ($gt > 1$), there are no exact analytical solutions, thus the numerical analysis has to be applied. We have used two methods to study the quantum dynamics: (i) the well-known Hamiltonian diagonalization proposed by Walls and Barakat [24] and (ii) the method of global characteristics based on manipulation with spectra [23]. These methods can be applied for arbitrary initial photon statistics. Nevertheless, for the purpose of our paper, we restrict our analysis to the initial coherent fields solely. Due to computational difficulties, the results can be obtained for small numbers of interacting photons only. The analysis of about one hundred interacting photons reaches practically the computational capabilities of the standard mathematical software.

Analysis of a typical evolution of the Fano factors $F_{1,2}^{\rm Q}$, such as presented in Fig. 1.1(a), leads to the conclusion that after initial short-time ($gt < 1$) relaxations in

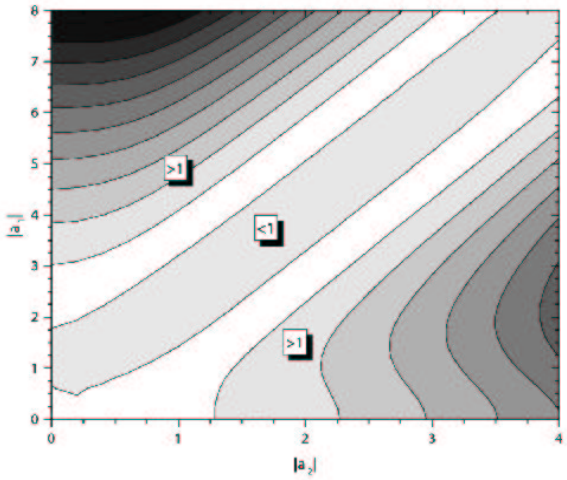

Fig. 1.2 Global Fano factor, F_2^{G}, of the second-harmonic mode as a function of the initial coherent state amplitudes α_1 and α_2 with $\theta = 0$. It is seen that the harmonic mode exhibits globally sub-Poissonian behavior ($F_2^{\mathrm{G}} < 1$) near the diagonal $|\alpha_1| = 2|\alpha_2|$ and $\theta = 0$. The darker region the higher value of F_2^{G}. The counter lines are drawn at $F_2^{\mathrm{G}} = 1, 1.5, \cdots, 5.5$.

both modes, a strongly super-Poissonian ($F_{1,2}^{\mathrm{Q}} \gg 1$). This behavior occurs for the majority of initial coherent states $|\alpha_1\rangle$ and $|\alpha_2\rangle$ except a certain set of initial states concentrated along the line $|\alpha_1| = 2|\alpha_2| > 0$ and $\theta \simeq 0$ [see Fig. 1.1(b)]. The same conclusion can be drawn by analyzing the global Fano factors $F_{1,2}^{\mathrm{G}}$. We find that the global Fano factor of the harmonic mode remains independent of amplitude $|\alpha_k|$ and equal to $F_2^{\mathrm{G}} = 0.83 < 1$ along the line $|\alpha_1| = 2|\alpha_2|$ (see Figs. 1.2 and 1.3). As depicted in Fig. 1.1(b), when the initial relaxation oscillations fade out, the harmonic mode remains sub-Poissonian for a long interaction time interval. In the classical theory of SHG, this case is referred to as the no-energy-transfer regime [25], because of the conservation of energy in every mode. We have found a quantum analog of this regime for coherent inputs with amplitudes satisfying the conditions: $|\alpha_1| = 2|\alpha_2|$ and $\theta \simeq 0$.

By analyzing Figs. 1.2 and 1.3, an intriguing question arises: Why does the harmonic-field photocount statistics in the no-energy-transfer regime remain sub-Poissonian with the Fano factor almost independent of the interaction time $gt > 1$? This behavior can be understood better by plotting the Husimi Q-function. Let us have a look at the snapshots of typical evolution of Q-functions for both modes at six times $gt = 0, 0.5 \cdots, 2.5$ with initial amplitudes $\alpha_1 = 6, \alpha_2 = 3$ (Fig. 1.4). These results were obtained numerically and represent the exact quantum solution of the model (1.5). One can observe how the cross-sections of the Q-functions change from circles (for initially coherent fields) through crescents into rings. We note that both modes have relatively small photon-number variances and small Fano factors, $F_1^{\mathrm{Q}} \approx 1.50$ and $F_2^{\mathrm{Q}} \approx 0.83$ [see also Fig. 1.1(b)]. The ring shapes, once formed,

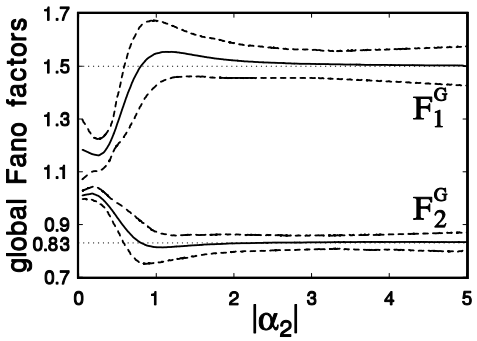

Fig. 1.3 Global Fano factors $F_1^{\rm G}$ and $F_2^{\rm G}$ along the line $|\alpha_1| = 2|\alpha_2|$ for $\theta = 0$. Dotted lines denote the RMS deviation of oscillations in the long-time interaction. It's seen that the harmonic mode exhibits globally sub-Poissonian behavior.

are very stable. So, not only the Fano factors, but the entire quantum states become stationary.

The Q-functions are very wide, thus no linearization of the quantum problem is possible and no pure quantum technique can be used for estimation of the observed values $F_1^{\rm Q} \approx 1.50$ and $F_2^{\rm Q} \approx 0.83$. However, good quantitative explanation of these numerical values can be obtained by the method of classical trajectories as will be shown in Sect. 1.2.3.

Our discussion is focused on photon-number statistics rather than squeezing or other phase-related properties. Nevertheless, by analyzing the Q-function evolution presented in Fig. 1.4, we can draw the conclusion that squeezing cannot be observed for initial coherent fields at interaction times exceeding the relaxation time. In fact, the quadrature squeezing variances ($k = 1, 2$)

$$S_k^{\rm Q} \equiv \langle (\Delta \hat{X}_k)^2 \rangle = \langle [\Delta (\hat{a}_k {\rm e}^{-{\rm i}\theta} + \hat{a}_k^\dagger {\rm e}^{{\rm i}\theta})]^2 \rangle \tag{1.9}$$

are monotonically rising from the standard shot-noise-limit ($S_k^{\rm Q} = 1$) to much more noisy state with the saturated quadrature variances

$$\begin{aligned} S_1^{\rm Q} &= 1 + 8r^2 \gg 1, \\ S_2^{\rm Q} &= 1 + 2r^2 \gg 1. \end{aligned} \tag{1.10}$$

It is evident that the no-energy-transfer regime is not useful for the quadrature squeezing generation.

1.2.2 Classical analysis

Complete quantum solution of the model given by Hamiltonian (1.5) can be found by applying sophisticated numeric methods on a fast computer only. However, since we

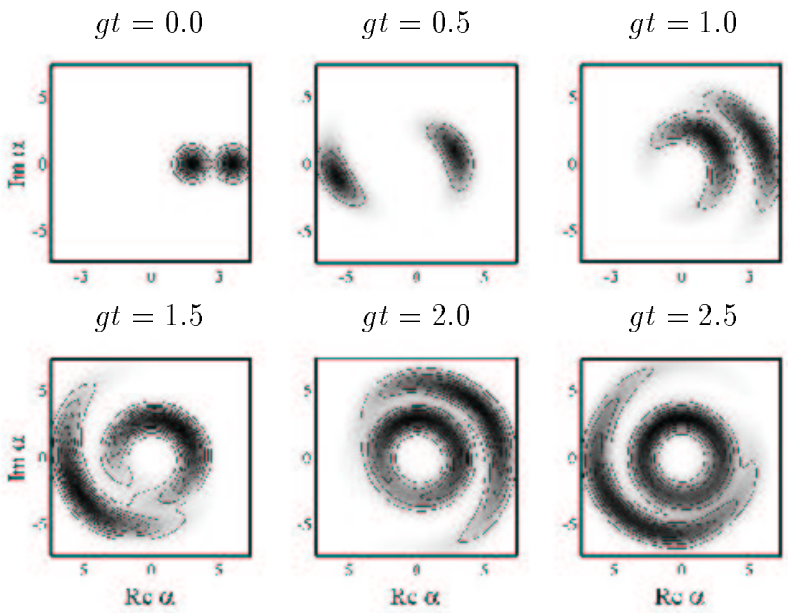

Fig. 1.4 Quantum evolution of the Q-function for the fundamental (outer contour plots) and the second-harmonic mode (inner plots) at six time moments for initial coherent states with $\alpha_1 = 6, \alpha_2 = 3, \theta = 0$. Solution obtained by quantum numerical method.

are interested in a special type of solution for strong fields, we can adopt approximate classical and semiclassical methods to obtain some analytical results.

In analogy with Eq. (1.5), the classical model of SHG can be described by

$$\mathcal{H} = g\left[\alpha_1^2\alpha_2^* + (\alpha_1^*)^2\alpha_2\right], \tag{1.11}$$

where α_1 and α_2 are complex amplitudes of the fundamental and second-harmonic modes, respectively, and g is a nonlinear coupling parameter. The exact solution of the model, described by (1.11), is well-known (see, e.g., [26]). The solution is periodic and can be written in terms of the Jacobi elliptic function. A few special cases (e.g., the phase-matched second-harmonic generation) have monotonous solution described by hyperbolic functions. The classical solution is a good approximation for strong fields, for which gives correct predictions of the output light intensities and frequency-conversion efficiency. Unfortunately, it cannot be used to describe the photocount noise and other statistical properties of generated light. Now, we will summarize some classical results, which we will be used in the method of classical trajectories.

The Hamiltonian (1.11) for the classical SHG leads to the following system of complex differential equations [26]

$$\dot{\alpha}_1 \quad = \quad -2\mathrm{i}g\alpha_1^*\alpha_2,$$

$$\dot{\alpha}_2 \;=\; -\mathrm{i}g\alpha_1^2. \tag{1.12}$$

One obtains, after substitution of $\alpha_k = r_k \mathrm{e}^{\mathrm{i}\phi_k}$, a new system of real equations for the amplitudes and phases:

$$\begin{aligned} \dot{r}_1 &= -2r_1 r_2 \sin\theta, \\ \dot{r}_2 &= r_1^2 \sin\theta, \\ \dot{\theta} &= \left(r_1^2/r_2 - 4r_2\right)\cos\theta, \end{aligned} \tag{1.13}$$

where $\theta = 2\phi_1 - \phi_2$. The system has two integrals of motion: $E = r_1^2 + 2r_2^2 = n_1 + 2n_2$ and $\Gamma = r_1^2 r_2 \cos\theta$. By extracting r_1 and θ from Eq. (1.13), we get the following equation for r_2:

$$\left(r_2\dot{r}_2/g\right)^2 + \Gamma^2 = r_2^2\left(E - 2r_2^2\right)^2, \tag{1.14}$$

or even in simpler form for the intensity $n_2 = r_2^2$:

$$\left(\dot{n}_2/2g\right)^2 + \Gamma^2 = n_2\left(E - 2n_2\right)^2. \tag{1.15}$$

Separation of t and n_2 leads to the equation

$$2g\mathrm{d}t = \frac{\mathrm{d}n_2}{\sqrt{n_2\left(E - 2n_2\right)^2 - \Gamma^2}}, \tag{1.16}$$

which can be rewritten as

$$4g\mathrm{d}t = \frac{\mathrm{d}n_2}{\sqrt{\left(a - n_2\right)\left(b - n_2\right)\left(n_2 - c\right)}}. \tag{1.17}$$

where the numbers a, b, c are the roots of cubic equation $n_2\left(E - 2n_2\right)^2 - \Gamma^2 = 0$. For $c \le u \le b < a$, the solution of Eq. (1.17) reads as

$$\int_c^u \frac{dx}{\sqrt{\left(a - x\right)\left(b - x\right)\left(x - c\right)}} = \frac{2}{\sqrt{a - c}}\,\mathrm{asn}\left(\sqrt{\frac{u - c}{b - c}}, k\right) \tag{1.18}$$

in terms of the inverse Jacobi elliptic function, $\mathrm{asn}\left(x, k\right)$, with parameter $k = \sqrt{\frac{b-c}{a-c}}$. Finally, the inversion of (1.18), gives the required solution

$$n_2\left(t\right) = c + \left(b - c\right)\,\mathrm{sn}^2\left[2g\sqrt{a - c}\left(t - t_0\right), k\right], \tag{1.19}$$

where $\mathrm{sn}(u, k)$ is the Jacobi elliptic function with the same parameter k. Solution (1.19) can be simplified in special cases. In particular, the well-known elementary solution is obtained for second-harmonic generation from vacuum, where $r_1\left(0\right) = r$ and $r_2\left(0\right) = 0$. In this case $k = 1$ and the Jacobi elliptic function simplifies to

hyperbolic tangent. Thus, the solution reads as

$$\begin{aligned} r_1(t) &= r\cosh(\sqrt{2}rgt), \\ r_2(t) &= \frac{r}{\sqrt{2}}\tanh(\sqrt{2}rgt) \end{aligned} \tag{1.20}$$

and $\theta(t) = \pi/2$. Subharmonic generation does not occur in this classical model, since for $r_1(0) = 0$ and $r_2(0) = r$ implies that $r_1(t) = 0,\ r_2(t) = r$ for any evolution time t. Another important special case of solution (1.19) can be obtained for the initial zero phase difference, $\theta(0) = 0$, and the initial amplitudes satisfying $r_1(0) = 2r$ and $r_2(0) = r$. Here, $E = 6r^2,\ \Gamma = 4r^3,\ a = 4r^2,\ b = c = r^2,\ k = 0$ and Jacobi elliptic function simplifies to trigonometric sinus. Finally, this elementary solution reads as

$$\begin{aligned} \alpha_1(t) &= 2re^{-2irgt}, \\ \alpha_2(t) &= re^{-4irgt}, \end{aligned} \tag{1.21}$$

which corresponds to the no-energy-transfer regime, in which energy is conserved in every mode. Phase trajectories of that solution are presented in Fig. 1.5(a). The slightly perturbed solution in the no-energy-transfer regime can also be approximated by $k \approx 0$ and elementary function sinus with small amplitude $(b - c) \approx 0$ [see Fig. 1.5(b),(c)].

1.2.3 Classical trajectory analysis

The answer to our question concerning the origin of sub-Poissonian behavior can be found by the method of classical trajectories. The method is very general. It can be applied in the analysis of almost every nonlinear quantum process. Even external pumping and energy losses can be easily described. In the classical trajectory approach to SHG [27], deterministic solutions of the classical SHG are used, while quantum noise of initial fields is artificially simulated by Gaussian distribution. One can study the time evolution of the bunch of trajectories like the evolution of quantum distributions. This semiclassical method can often shed some light on complicated quantum dynamics. For strong inputs, where the quantum noise can be assumed small, the method gives surprisingly good results.

According to the classical trajectory method, one assumes that the input stochastic amplitudes are of the form

$$\begin{aligned} \alpha_1 &= r_1 + x_1 + \mathrm{i}y_1, \\ \alpha_2 &= r_2 + x_2 + \mathrm{i}y_2, \end{aligned} \tag{1.22}$$

where r_k are coherent complex amplitudes, whereas x_k and y_k are real and mutually independent Gaussian stochastic quantities with identical variances

$$\sigma^2 = 1/4 \ll r_k^2. \tag{1.23}$$

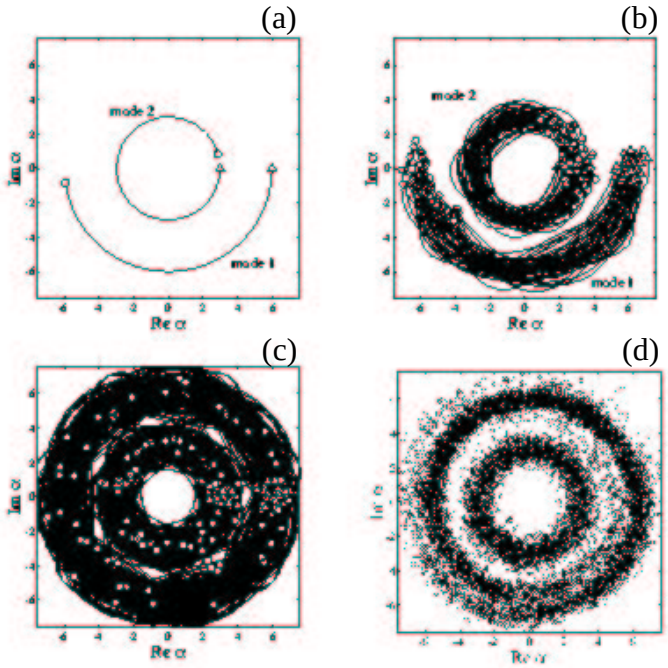

Fig. 1.5 Classical trajectories of the fundamental and second-harmonic modes in the no-energy-transfer regime for $\alpha_1 = 6$ and $\alpha_2 = 3$: **(a)** classical evolution according to Eq. (1.19) for $0 < gt < 0.5$; **(b)** fifty random trajectories out of 10,000 trajectories used in the simulations for $0 < gt < 0.5$; **(c)** same as in (b), but for $0 < gt < 5$; **(d)** snapshot of the Q-function, obtained from 10,000 random trajectories at time $gt = 5.0$. Triangles denote starting points ($gt = 0$) of the trajectories and circles are their ends.

By analogy with our quantum analysis, we calculate the semiclassical Fano factor, defined by Eq. (1.4), and quadrature squeezing variance

$$S_k^{\mathrm{S}} \equiv \overline{(\Delta X_k)^2} = \overline{[\Delta(\alpha_k \mathrm{e}^{-\mathrm{i}\theta} + \alpha_k^* \mathrm{e}^{\mathrm{i}\theta})]^2} \tag{1.24}$$

as counterparts of quantum parameters (1.1) and (1.9), respectively. By applying the method of classical trajectories with the noise variance given by Eq. (1.23), we find the semiclassical quadrature squeezing and Fano factor given by:

$$\begin{aligned} S_k^{\mathrm{S}} &= 4\sigma^2 = 1, \\ F_k^{\mathrm{S}} &\approx 4\sigma^2 = 1, \end{aligned} \tag{1.25}$$

respectively. According to the described method, one needs to solve thousands of the classical SHG trajectories. The mean values are simply obtained by averaging over all these trajectories. In Fig. 1.6, we have presented graphically snapshots in a selected time-interval of all complex solutions in phase space. These clouds of points naturally correspond to the Q-functions in the quantum picture (see Fig. 1.4). We have found that this semiclassical method gives the results surprisingly similar

to the quantum results even for relatively weak fields! This very good agreement is clearly seen by comparing Figs. 1.4 and 1.6, where the initial amplitudes are chosen to be $\alpha_1 = 6$, $\alpha_2 = 3$. The patterns given by fifty random trajectories out of the total number of 10,000 analyzed trajectories are shown in Fig. 1.5(b) in the time interval $gt \in (0, 0.5)$ and Fig. 1.5(c) in $gt \in (0, 5)$. The final snapshot of the "cloud" ring at $gt = 5$ is given in Fig. 1.5(d).

The method of classical trajectories can be used not only numerically (Figs. 1.5 and 1.6) but also analytically in special cases. For example, the evolution of low-noise fields in the no-energy-transfer regime can be found analytically in the first approximation with the solution given by elementary trigonometric functions. To show this, let us analyze integrals of motions. On assuming the initial amplitudes of the form $\alpha_1 = 2r + x_1 + iy_1$ and $\alpha_2 = r + x_2 + iy_2$, the integrals of motion can be expressed in the form of successive corrections

$$\begin{aligned} E &= 6r^2 + \Delta E_1 + \Delta E_{0,} \\ \Gamma &= 4r^3 + \Delta\Gamma_2 + \Delta\Gamma_1 + \Delta\Gamma_0, \end{aligned} \tag{1.26}$$

where we denote $\Delta E_1 = 4r\left(x_1 + x_2\right)$, $\Delta E_0 = x_1^2 + y_1^2 + 2\left(x_2^2 + y_2^2\right)$, and $\Delta\Gamma_2 = 4r^2\left(x_1 + x_2\right)$, $\Delta\Gamma_1 = r\left(x_1^2 - y_1^2 + 4x_1x_2\right)$ and $\Delta\Gamma_0 = x_2\left(x_1^2 - y_1^2\right) + 2x_1y_1y_2$. By substituting $n_2 = E/6 + \epsilon$, where ϵ is a small correction, and after omitting the cubic term $2\epsilon^3$, we find that the denominator in Eq. (1.16) can be approximated by the quadratic function

$$n_2\left(E - 2n_2\right)^2 - \Gamma^2 \approx 2E\left(A^2 - \epsilon^2\right). \tag{1.27}$$

Now, we can perform integration of these elementary functions leading to the simple result

$$n_2(t) = r^2 + B + A\cos\Omega gt, \tag{1.28}$$

where $\Omega = \sqrt{8E}$, $A = \frac{2}{3}r\sqrt{\left(x_1 - 2x_2\right)^2 + 3\left(y_1^2 + y_2^2\right)}$ and $B = \frac{2}{3}r\left(x_1 + x_2\right)$. We get a similar result

$$n_1(t) = E - 2n_2 = 4r^2 + 4B - 2A\cos\Omega gt \tag{1.29}$$

for the fundamental (or subharmonic) mode. Both solutions are constant functions weakly perturbed by harmonic function. The evolution in phase space can be understood clearly by analyzing Figs. 1.5 and 1.6. Due to the frequency dispersion $\Omega\left(\{x_k, y_k\}\right)$ [see Fig. 1.5(b),(c)], different trajectories are drifting variously and create a crescent-shape cloud in phase space, which develops later into a full ring as seen in Figs. 1.5 and 1.6. One has to perform the averaging of solutions to calculate the required statistical moments. We find $\overline{n}_1 = 4r^2$, $\overline{n}_2 = r^2$, and

$$\begin{aligned} \overline{n_1^2} &= 16r^4 + 16\overline{B^2} + 2\overline{A^2}, \\ \overline{n_2^2} &= r^4 + \overline{B^2} + \frac{1}{2}\overline{A^2}, \end{aligned} \tag{1.30}$$

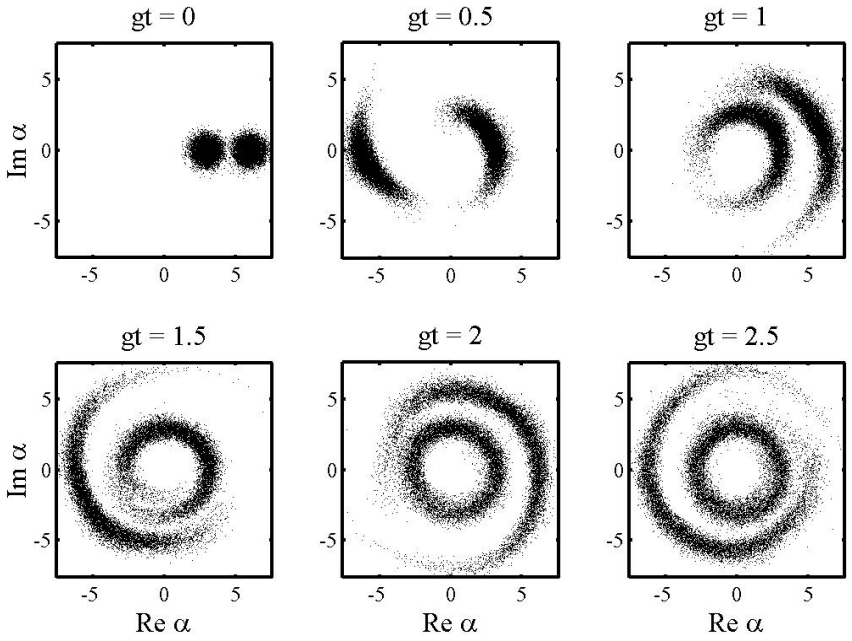

Fig. 1.6 Classical trajectory simulation of quantum evolution of the Q-function for the same initial conditions and interaction times as in Fig. 1.4. In our simulation 10,000 trajectories were calculated.

where $\overline{B} = 0$, $\overline{A^2} = \frac{44}{9}r^2\sigma^2 = \frac{11}{9}r^2$, $\overline{B^2} = \frac{8}{9}r^2\sigma^2 = \frac{2}{9}r^2$ and $\overline{\cos^2 \Omega gt} = \frac{1}{2}$. Finally, we arrive at the semiclassical Fano factors given by simple rational numbers:

$$\begin{aligned} F_1^{\mathrm{S}} &= \frac{1}{r^2}\left(4\overline{B^2} + \frac{1}{2}\overline{A^2}\right) = \frac{3}{2}, \\ F_2^{\mathrm{S}} &= \frac{1}{r^2}\left(\overline{B^2} + \frac{1}{2}\overline{A^2}\right) = \frac{5}{6}. \end{aligned} \tag{1.31}$$

By analyzing Figs. 1.1(b) and 1.3 as well as tables 1.1 and 1.2, we conclude that our estimations (1.31) are in very good agreement with those values of Fano factors obtained by the quantum numerical analysis of Sect. 1.2.2.

1.3 HIGHER-HARMONIC GENERATION

1.3.1 Quantum analysis

In this section, we will generalize our results of Sect. 1.2 to describe the processes of the N-th harmonic generation. Again, we will focus on predictions of the sub-Poissonian photon-number statistics.

Processes of the N-th harmonic or subharmonic generation can be described by the conventional interaction Hamiltonian (e.g., [5])

$$\hat{H} = \hbar g \left(\hat{a}_1^N \hat{a}_N^\dagger + \hat{a}_1^{\dagger N} \hat{a}_N \right) \tag{1.32}$$

for $N = 2, 3, \cdots$. In (1.32), $\hat{a}_1$ and $\hat{a}_N$ denote annihilation operators of the fundamental and N-th harmonic modes, respectively, and g is a nonlinear coupling parameter. For short evolution times, the following approximation of the quantum Fano factors can be obtained for the fundamental mode [13]

$$F_1^{\mathrm{Q}} = 1 - 2N\left(N-1\right) r_1^{N-2} r_2 \sin\theta \; gt + \mathcal{O}\{(gt)^2\} \tag{1.33}$$

with $N = 2, 3, \ldots$, and for higher harmonics:

$$\begin{aligned} F_3^{\mathrm{Q}} &= 1 - 36 r_1^3 r_2 \left(r_1^2 + 2\right) \sin\theta \; (gt)^3 + \mathcal{O}\{(gt)^4\}, \\ F_4^{\mathrm{Q}} &= 1 - 64 r_1^4 r_2 \left(17 + 12 r_1^2 + 2 r_1^4\right) \sin\theta \; (gt)^3 + \mathcal{O}\{(gt)^4\}, \end{aligned} \tag{1.34}$$

where r_k are input amplitudes, and $\theta = N\phi_1 - \phi_N$ is the input phase mismatch. For spontaneous harmonic generation (i.e., for $r_N = 0$), Eqs. (1.33)-(1.34) simplify to the formulas derived by Kozierowski and Kielich [14]. This analysis shows the possibility of sub-Poissonian light generation in short-time regime under the proper phase condition.

On testing different coherent input amplitudes and phases in order to minimize the Fano factor for long-interaction times, we have discovered a regime, for which the harmonic field exhibits the quasi-stationary sub-Poissonian photocount noise. The regime occurs if the ratio of amplitudes $|\alpha_1|$ and $|\alpha_N|$ is equal to N, and phases are related by $N\phi_1 = \phi_N$. As described in Sect. 1.2 for SHG, this is a quantum analog of the no-energy-transfer regime [25] known from classical nonlinear optics as an evolution exhibiting the no-energy transfer between the interacting modes. The intensities of both modes remain quasi-stationary during the interaction. Obviously, in quantum analysis some small energy fluctuations between modes are observed as a consequence of vacuum fluctuations. However, the influence of energy fluctuations can be neglected for strong fields.

For better comparison of theoretical predictions for different order processes, we have plotted the quantum Fano factors for both interacting modes in the no-energy-transfer regime with $N = 2 - 5$ and $r = 5$ in Fig. 1.7. One can see that all curves start from $F_{1,N}^{\mathrm{Q}}(0) = 1$ for the input coherent fields and become quasi-stationary

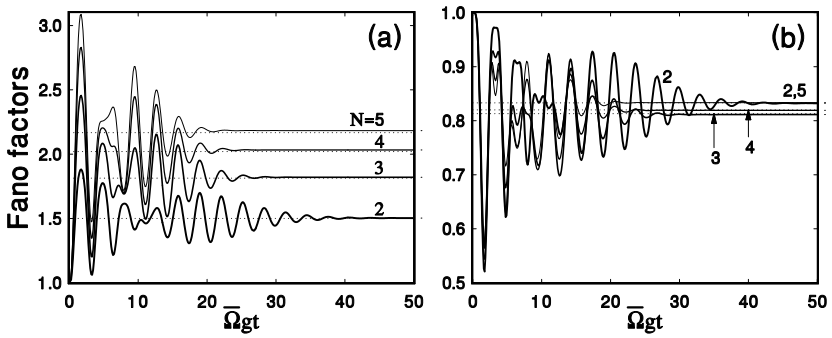

Fig. 1.7 Time evolution of the exact quantum Fano factors: **(a)** $F_1^{\mathrm{Q}} = F_1^{\mathrm{Q}}(N)$ for the fundamental mode and **(b)** F_N^{Q} for the harmonic mode in Nth-harmonic generation for N=2 (thickest curve), 3, 4, and 5 (thinnest curve). Time t is rescaled with frequency $\overline{\Omega}$, given by (1.52), and coupling constant g. The harmonic-mode amplitude is $r = r_N = 5$. The dotted lines correspond to the semiclassical Fano factors, given by (1.54) and (1.55). It is seen that the fundamental mode is super-Poissonian, whereas the harmonic mode is sub-Poissonian for all non-zero evolution times.

after some relaxations. The quantum and semiclassical Fano factors coincide for high-intensity fields and longer times, specifically for $t \geq 50/(\overline{\Omega}g)$, where $\overline{\Omega}$ will be defined later by Eq. (1.54). In Fig. 1.7, we observe that all fundamental modes remain super-Poissonian ($F_1^{\mathrm{Q}}(t) > 1$), whereas the Nth harmonics become sub-Poissonian ($F_N^{\mathrm{Q}}(t) < 1$). The most suppressed noise is observed for the third harmonic with the Fano factor $F_3^{\mathrm{Q}} \approx 0.81$. In Fig. 1.7, we have included the predictions of the classical trajectory method (plotted by dotted lines) to show that they properly fit the exact quantum results (full curves) for the evolution times $t \geq 50/(\overline{\Omega}g)$. The small residual differences result from the fact that the amplitude r was chosen to be relatively small ($r = 5$). This value does not precisely fulfill the condition $r \gg 1$. We have taken $r = 5$ as a compromise between the asymptotic value $r \to \infty$ and computational complexity to manipulate the matrices of dimensions 1000×1000. Unfortunately, we cannot increase amplitude r arbitrary due to computational limitations. Numerical values of the quantum Fano factors in comparison with their semiclassical approximations for the fundamental mode, given by Eq. (1.56), are presented in their dependence on N in table 1.1 and Fig. 1.8(a). Analogously, those values for harmonics are presented in Fig. 1.8(b) and table 1.2 as calculated by the numerical quantum method and from analytical semiclassical formula (1.57). It is seen that the approximate predictions of the Fano factors, according to (1.56) and (1.57), fit very well the values obtained by applying the numerical quantum method. In fact, the differences between the approximate and exact values are hardly visible on the scale of Fig. 1.8. Nevertheless, some small ($< 1\%$) differences in $F_{1,N}^{\mathrm{Q}}$ (see tables 1.1 and 1.2) can be explained by the fact that the value of r for numerical analysis was chosen too small.

1.3.2 Classical analysis

Our classical analysis of higher-harmonic generation follows the same method as described in Sect. 1.2.3. The classical model of the Nth-harmonic generation can be described by

$$\mathcal{H} = g\left[\alpha_1^N \alpha_N^* + (\alpha_1^*)^N \alpha_N\right], \tag{1.35}$$

which in a special case of $N = 2$ goes over into Eq. (1.11). In Eq. (1.35), α_1 (α_N) is the complex amplitude of the fundamental (Nth-harmonic) mode. Hamiltonian (1.35) leads to the pair of complex differential equations [26]

$$\begin{aligned} \dot{\alpha}_1 &= -\mathrm{i}gN\alpha_1^{*N-1}\alpha_N, \\ \dot{\alpha}_N &= -\mathrm{i}g\alpha_1^N, \end{aligned} \tag{1.36}$$

On introducing real amplitudes and phases, $\alpha_k = r_k \mathrm{e}^{\mathrm{i}\phi_k}$, (1.36) can be transformed into the system of three real equations:

$$\begin{aligned} \dot{r}_1 &= -gNr_1^{N-1} r_N \sin\theta, \\ \dot{r}_N &= gr_1^N \sin\theta, \end{aligned}$$

Table 1.1 Quasi-stationary values of the quantum Fano factors F_1^{Q} and their semiclassical approximations F_1^{S}, given by (1.54), for the fundamental mode in Nth-harmonic generation with $N = 1 - 5$ in the no-energy-transfer regime. The values of F_1^{Q} are calculated for $r = r_N = 5$.

N	F_1^{Q}	F_1^{S}	$(F_1^{\mathrm{Q}} - F_1^{\mathrm{S}})/F_1^{\mathrm{Q}}$
1	1	1	0
2	1.5029291	3/2	0.0020
3	1.8202032	29/16	0.0042
4	2.0323293	101/50	0.0061
5	2.1830414	13/6	0.0075

Table 1.2 Same as in table 1, but for the Nth harmonic mode; F_N^{S} are calculated from (1.55).

N	F_N^{Q}	F_N^{S}	$\lvert F_N^{\mathrm{Q}} - F_N^{\mathrm{S}}\rvert/F_N^{\mathrm{Q}}$
1	1	1	0
2	0.83228800	5/6	0.0013
3	0.81125970	13/16	0.0015
4	0.81924902	41/50	0.00092
5	0.83331127	5/6	0.000026

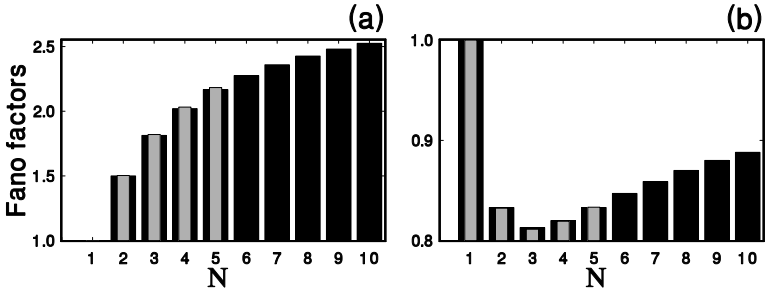

Fig. 1.8 Semiclassical (solid bars) and quantum (dithered bars) Fano factors versus order N of harmonic generation for **(a)** fundamental and **(b)** Nth-harmonic modes in the quasi-stationary no-energy-transfer regime. Figures (a) and (b) for $N = 1 - 5$ correspond to tables 1 and 2, respectively. It is seen that the quantum results are well fitted by the semiclassical Fano factors. According to both analyses, the third-harmonic mode has the most suppressed photocount noise.

$$\dot{\theta} \quad = \quad g\left(r_1^N / r_N - N^2 r_1^{N-2} r_N\right) \cos\theta, \tag{1.37}$$

where $\theta = N\phi_1 - \phi_N$ is the phase mismatch. Equations (1.37) have two integrals of motion:

$$\begin{aligned} E &= r_1^2 + N r_N^2 = n_1 + N n_N, \\ \Gamma &= r_1^N r_N \cos\theta. \end{aligned} \tag{1.38}$$

On extraction of r_1 and θ from Eq. (1.37), we find equation for the amplitude r_N:

$$\left(r_N \dot{r}_N / g\right)^2 + \Gamma^2 = r_N^2 \left(E - N r_N^2\right)^N \tag{1.39}$$

or its simpler form for the intensity $n_N = r_N^2$:

$$\left(\dot{n}_N / 2g\right)^2 = n_N \left(E - N n_N\right)^N - \Gamma^2. \tag{1.40}$$

The general solution for $n_N\,(t)$ is a periodic function oscillating between the values $n_{\min}$ and $n_{\max}$. The solution can be given in terms of the Jacobi elliptic functions for $N = 2$ and $N = 3$, and in terms of hyperelliptic functions for $N > 3$.

One elementary solution of set of Eqs. (1.37) is obtained for the zero initial phase mismatch $\theta = 0$ and the initial amplitudes satisfying the condition $r_1 = N r_N$. The solution reads as

$$\begin{aligned} \alpha_1\,(t) &= r_1 \exp(-\mathrm{i} g t r_1^{N-1}), \\ \alpha_N\,(t) &= r_N \exp\left(-\mathrm{i} N g t r_1^{N-1}\right), \end{aligned} \tag{1.41}$$

which corresponds to the no-energy-transfer regime, since the amplitude and energy in both the interacting modes remain constant $n_1\,(t) = |\alpha_1\,(t)|^2 = r_1^2$ and $n_N\,(t) = |\alpha_N\,(t)|^2 = r_N^2$ [25].

1.3.3 Classical trajectory analysis

The results of Sect. 1.3.2 can be used in the method of classical trajectories in analogy with the technique described in Sect. 1.2.3. We need to express the trajectories in their dependence on small noise parameters x_k and y_k. The integrals of motion, given by (1.38), can be expressed in a form of corrections in successive powers of large r:

$$E = N\left(N+1\right)r^2 + \Delta E_1 + \Delta E_0, \tag{1.42}$$

where

$$\begin{aligned} \Delta E_1 &= 2N\left(x_1 + x_N\right)r, \\ \Delta E_0 &= x_1^2 + y_1^2 + N\left(x_N^2 + y_N^2\right), \end{aligned} \tag{1.43}$$

and

$$\Gamma = N^N r^{N+1} + \Delta\Gamma_N + \Delta\Gamma_{N-1} + \Delta\Gamma_{N-2} + \cdots, \tag{1.44}$$

where

$$\begin{aligned} \Delta\Gamma_N &= \left(x_1 + x_N\right)\left(Nr\right)^N, \\ \Delta\Gamma_{N-1} &= \left[\frac{N-1}{2}\left(x_1^2 - y_1^2\right) + N\left(x_1 x_N + y_1 y_N\right)\right]\left(Nr\right)^{N-1}. \end{aligned} \tag{1.45}$$

The lower-order terms $\Delta\Gamma_{N-2}$, $\Delta\Gamma_{N-3}$, $\cdots$ can be neglected in further considerations. On assumption of high-intensity fields ($r \gg 1$), we can substitute

$$n_N = \frac{E}{N\left(N+1\right)} + \epsilon, \tag{1.46}$$

where ϵ is a small correction of stationary value. Then, r.h.s. of (1.40) can be rewritten as

$$n_N\left(E - Nn_N\right)^N - \Gamma^2 \approx \frac{N^N}{2\left(N+1\right)^{N-2}} E^{N-1}\left(A^2 - \epsilon^2\right) \tag{1.47}$$

on omission of higher-order terms involving ϵ^3, ϵ^4, $\cdots$. One arrives at simple equation

$$\left(\frac{\dot{\epsilon}}{2g}\right)^2 = \frac{N^N}{2\left(N+1\right)^{N-2}} E^{N-1}\left(A^2 - \epsilon^2\right). \tag{1.48}$$

Thus, the solution of (1.40) reads as

$$n_N\left(t\right) = r^2 + B + A\sin\Omega g t, \tag{1.49}$$

where the frequency Ω is given by

$$\Omega = \sqrt{\frac{2N^N E^{N-1}}{(N+1)^{N-2}}} \tag{1.50}$$

and

$$\begin{aligned} A &= \frac{r}{N+1}\sqrt{4\left(x_1 - Nx_N\right)^2 + 2N\left(N+1\right)\left(y_1 - y_N\right)^2} \\ B &= \frac{\Delta E_1}{N\left(N+1\right)} = \frac{2}{N+1} r\left(x_1 + x_N\right). \end{aligned} \tag{1.51}$$

From (1.38), a result similar to (1.49) is obtained for the fundamental mode:

$$n_1\left(t\right) = E - Nn_N\left(t\right) = N^2 r^2 + N^2 B - NA\sin\Omega g t. \tag{1.52}$$

It is seen that both solutions (1.49) and (1.52) are given in a form of large constants weakly perturbed by harmonic function.

Now, on applying the classical trajectory method, one should perform averaging over all solutions (1.49) and (1.52) to calculate the required statistical moments. Here, we calculate the first and second-order field-intensity moments necessary for determination of the Fano factors. The mean intensities of the fundamental and harmonic modes are simply given by $\overline{n}_1 = N^2 r^2$ and $\overline{n}_N = r^2$, respectively. The second-order moments of field intensity are found to be

$$\begin{aligned} \overline{n_1^2} &= N^4 r^4 + N^4\overline{B^2} + \frac{1}{2}N^2\overline{A^2}, \\ \overline{n_N^2} &= r^4 + \overline{B^2} + \frac{1}{2}\overline{A^2}. \end{aligned} \tag{1.53}$$

in terms of $\overline{A^2} = r^2(2N^2+N+1)/(N+1)^2$ and $\overline{B^2} = 2r^2/(N+1)^2$. We note that $\overline{B}$ vanishes. The term $\overline{\sin^2\Omega g t}$ can simply be estimated with $1/2$ for sufficiently long time t, when $n_k\left(t\right)$ and $F_k^{\mathrm{Q}}\left(t\right)$ become quasi-stationary. The relaxation in $n_k\left(t\right)$ and $F_k^{\mathrm{Q}}\left(t\right)$ is observed for short times t due to the presence of harmonic sine function and residual phase synchronization. The mean value of the frequency (1.50), given by

$$\overline{\Omega} \approx \sqrt{2N\left(N+1\right)}\left(Nr\right)^{N-1}, \tag{1.54}$$

enables estimation of the oscillation period $T_{\mathrm{osc}} = 2\pi/\overline{\Omega}$, whereas the standard deviation

$$\Delta\Omega \approx \sqrt{2N\left(N+1\right)}N^{N-1}r^{N-2}\frac{N-1}{N+1} \tag{1.55}$$

determines the duration $T_{\mathrm{rel}} = 2\pi/\Delta\Omega$ of relaxation. By comparing the characteristic times T_{osc} and T_{rel}, one finds that the evolution time can be scaled by $\tau = \overline{\Omega} g t$ to synchronize optimally the oscillations of the exact quantum solutions for different

N. These synchronized oscillations of the Fano factors are clearly presented in Fig. 1.7.

Finally, we arrive at the semiclassical Fano factors

$$F_1^{\mathrm{S}} = \frac{1}{2}\frac{6N^2+N+1}{(N+1)^2}, \tag{1.56}$$

$$F_N^{\mathrm{S}} = \frac{1}{2}\frac{2N^2+N+5}{(N+1)^2}, \tag{1.57}$$

which are the compact-form analogs of the quantum Fano factors. The semiclassical Fano factors for the fundamental and higher harmonics for various values of N are listed in tables 1.1 and 1.2, and plotted in Figs. 1.7(a) and 1.7(b), respectively.

Our solutions (1.56) and (1.57) reduce to the results derived in Ref. [19] for $N = 2$, and those of Ref. [20] for $N = 3$. By analyzing (1.57), we find that higher harmonics evolve into quasi-stationary sub-Poissonian states ($F_N^{\mathrm{S}} < 1$) for any $N > 1$. Except for second harmonic, the photocount noise reduction in higher harmonics becomes less effective with increasing N. Thus, the deepest noise reduction occurs for the third harmonic as described by the Fano factor $F_3^{\mathrm{S}} = \frac{13}{16} = 0.8125$. The photocount noise reductions for the second and fifth harmonics are predicted to be the same, although the quantum analysis (see table 1.2) reveals that they differ slightly ($< 1\%$). As comes from (1.56), the fundamental mode has solely the super-Poissonian photocount statistics ($F_1^{\mathrm{S}} > 1$) with noise monotonically growing in N for the no-energy-transfer regime. For $N = 1$, the process is linear and no change in the photon statistics occurs. The interacting modes remain coherent with the unit Fano factors for both modes. It is worth noting that qualitatively different photocount statistics of the fundamental mode is observed in the short-interaction regime as given by Eqs. (1.6) and (1.33)-(1.34).

We have shown, in agreement with the results presented in [19], that the method of classical trajectories gives very good predictions in the case of strong-field interactions (i.e., for the photon numbers larger than 10). The calculation speed of the method does not depend on numbers of interacting photons. But better approximation is achieved with the increasing number of photons. Thus, the method is very fast and significantly simplifies the tedious exact quantum calculations.

1.4 CONCLUSION

We have presented quantum, classical and semiclassical descriptions of second and higher harmonic generations. We have demonstrated that these processes can be a source of sub-Poissonian light. On testing different coherent input amplitudes and phases in order to minimize the Fano factor, we have discovered a quantum regime for which the long-interaction output is generated with the quasi-stationary sub-Poissonian photocount noise [19, 20, 21]. The regime occurs if the initial coherent state amplitudes are related by $|\alpha_1| = N|\alpha_N|$ and $\mathrm{Arg}(\alpha_N) \simeq N\,\mathrm{Arg}(\alpha_1)$. This is a

quantum analog of the no-energy-transfer regime [25] known in classical nonlinear optics as an evolution exhibiting no-energy transfer between the interacting modes. The intensities of both modes remain quasi-constant in time during the interaction. Obviously, in a quantum analysis some small energy fluctuations between modes are observed as a consequence of vacuum fluctuations. However, the influence of energy fluctuations can be neglected for strong fields.

We have proved that in the no-energy-transfer regime, the fundamental mode evolves into a quasi-stationary state with the super-Poissonian ($F_1^{\mathrm{Q}} > 1$) photocount statistics, whereas the N-th harmonic goes over into a sub-Poissonian ($F_N^{\mathrm{Q}} < 1$) quasi-stationary state. We have found that the most suppressed photocount noise is obtained for the third harmonic as described by the quantum Fano factor $F_3^{\mathrm{Q}} = 0.811\cdots$. Good analytical predictions of the quantum Fano factors for both the fundamental and harmonic modes ($F_3^{\mathrm{S}} = 13/16 = 0.8125$) were obtained under the semiclassical approximation in the strong-field limit.

Acknowledgments

J.B. thanks Prof. Jan Peřina and Dr. Ondřej Haderka for interesting discussions. A.M. wishes to thank Professors Nobuyuki Imoto and Masato Koashi for their hospitality and stimulating research at SOKEN. J.B. was supported by the Ministry of Education of Czech Republic under Projects VS96028, CEZ J14/98 and LN00A015, and by the Grant Agency of Czech Republic (No. 202/00/0142). A.M. was supported by the Japan Science and Technology Corporation (JST-CREST).

REFERENCES

1. P. A. Franken, A. E. Hill, C. W. Peters and G. Weinreich, *Phys. Rev. Lett.* **7**, 118 (1961); M. Bass, P. A. Franken, J. F. Ward and G. Weinreich, *Phys. Rev. Lett.* **9**, 446 (1962).

2. N. Bloembergen, and P.S. Pershan, *Phys. Rev.* **128**, 606 (1962); J. A. Armstrong, N. Bloembergen, J. Ducuing and P.S. Pershan, *Phys. Rev.* **127**, 1918 (1962); N. Bloembergen *Nonlinear Optics*, Benjamin, New York, 1965.

3. S. Youn, S. Choi, P. Kumar and R. Li, *Opt. Lett.* **21**, 1597 (1996); R. Li, S. Choi, Ch. Kim and P. Kumar, *Phys. Rev.* A **51**, 3429 (1995); E. Sidick, A. Knoesen and A. Dienes, *J. Opt. Soc. Am. B* **12**, 1704 (1995); N. C. Kothari and X. Carlotti, *Opt. Soc. Am. B* **5**, 756 (1988).

4. L. Mandel and E. Wolf, *Optical Coherence and Quantum Optics*, chaps. 12.10 and 14.9., University Press., Cambridge, 1995.

5. J. Peřina, *Quantum Statistics of Linear and Nonlinear Optical Phenomena*, chap. 10., Kluwer, Dordrecht, 1991.

6. M. Kozierowski and R. Tanaś, *Opt. Commun.* **21**, 229 (1977).

7. S. Kielich, M. Kozierowski and R. Tanaś, *Coherence and Quantum Optics IV*, ed. L. Mandel and E. Wolf, page 511, Plenum, New York, 1978.

8. L. Mandel, *Opt. Commun.* **42**, 437 (1982).

9. C. K. Hong and L. Mandel, *Phys. Rev A* **32**, 974 (1982).

10. M. Hillery, *Opt. Comm.* **62**, 135 (1987).

11. J. Peřina, Z. Hradil, and B. Jurčo, *Quantum Optics and Fundamentals of Physics*, chap. 8.5. Kluwer, Dordrecht, 1994; H. A. Bachor, *A Guide to Experiments in Quantum Optics*, chap. 9., Wiley, Weinheim, 1998.

12. Y. P. Malakyan, *Opt. Commun.* **86**, 423 (1991).

13. J. Bajer and J. Peřina, *Opt. Commun.* **92**, 99 (1992).

14. M. Kozierowski and S. Kielich, *Phys. Lett.* **94**, 213 (1983).

15. J. Bajer, T. Opatrný and J. Peřina, *Quantum Opt.* **6**, 403 (1994).

16. M. Kozierowski, *Phys. Rev. A* **34**, 3474 (1986).

17. S. D. Du, C. D. Gong, *Phys. Rev. A* **48**, 2198 (1993).

18. Y. B. Zhan, *Phys. Rev. A* **46**, 686 (1992).

19. J. Bajer, O. Haderka and J. Peřina, *J. Opt. B: Quantum Semiclass. Opt.* **1**, 529 (1999).

20. J. Bajer, O. Haderka, J. Peřina and A. Miranowicz, *Czech. J. Phys.* **50**, 717 (2000).

21. J. Bajer and A. Miranowicz, *J. Opt. B: Quantum Semiclass. Opt.* **2**, L10 (2000).

22. U. Fano, *Phys. Rev.* **72**, 26 (1947).

23. O. Haderka, J. Bajer, J. Peřina, *Quantum Semiclass. Opt.* **8**, 1159 (1996).

24. D. Walls and R. Barakat, *Phys. Rev. A* **1**, 446 (1970).

25. H. Paul, *Nichtlineare Optik II*, page 16, Academie, Berlin, 1973; A. Bandilla, G. Drobný and I. Jex, *Opt. Comm.* **128**, 353 (1996); G. Drobný, A. Bandilla and I. Jex, *Phys. Rev. A* **55**, 78 (1997).

26. R. W. Boyd, *Nonlinear Optics*, page 78, Academic Press, 1991; A. Bandilla, G. Drobný and I. Jex, *Opt. Comm.* **156**, 112 (1998).

27. S. P. Nikitin and A. V. Masalov, *Quantum. Opt.* **3**, 105 (1991); G. J. Milburn, *Phys. Rev. A* **33**, 674 (1986).